

# Pulsed extraction of ionization from helium buffer gas

D.J. Morrissey<sup>a,b,\*</sup>, G. Bollen<sup>a,c</sup>, M. Facina<sup>a</sup>, S. Schwarz<sup>a</sup>

<sup>a</sup>*National Superconducting Cyclotron Laboratory,*

<sup>b</sup>*Department of Chemistry,*

<sup>c</sup>*Department of Physics and Astronomy,  
Michigan State University, East Lansing MI 48824*

---

## Abstract

The migration of intense ionization created in helium buffer gas under the influence of applied electric fields is considered. First the chemical evolution of the ionization created by fast heavy-ion beams is described. Straight forward estimates of the lifetimes for charge exchange indicate a clear suppression of charge exchange during ion migration in low pressure helium. Then self-consistent calculations of the migration of the ions in the electric field of a gas-filled cell at the National Superconducting Cyclotron Laboratory (NSCL) using a Particle-In-Cell computer code are presented. The results of the calculations are compared to measurements of the extracted ion current caused by beam pulses injected into the NSCL gas cell.

*Key words:* Nuclear recoils, helium buffer gas, Ion transport by electrostatic fields, Space charge, Radioactive ion beams

*PACS:* 29.25.Rm, 29.40.Cs, 41.85.Ar, 52.25.Vy

---

## 1. Introduction

The thermalization of nuclear reaction products in a buffer gas for subsequent extraction and study is an active area of research. Thermalization provides very-low energy beams of short-lived isotopes that can be used for precision mass measurements in traps [1,2,3], for laser-spectroscopy[4], or be (re)accelerated to higher energies for reaction and nuclear spectroscopic studies[5,6]. The products may be from high-energy nuclear reactions with mass selection before entering the gas [7,8] or be from low-energy nuclear reactions and fly directly into the gas [9,10,11,12,13]. The key requirement on all of these

---

\* Corresponding author

*Email address:* morrissey@nscl.msu.edu (D.J. Morrissey).

systems is that the fast reaction products must be rapidly and efficiently converted into high-quality, low-energy beams (kinetic energy  $\sim$ eV). However, the simple stopping of each nuclear recoil in the buffer gas creates from  $10^4$  to  $10^7$  ion-electron pairs (the primary ionization) that will hinder the collection of the single incident ion.

There are a number of detailed reports of the extraction of nuclear reaction products from gas cells with a variety of geometries and gas pressures using electric fields [7,10,11,12] and without electrodes[13,9]. The gas cells with electric fields rely on separating the ion-electron pairs and drifting the cations to the exit nozzle (the more mobile electrons are expected to be collected rapidly at the other end of the chamber). These gas cells work in a weak plasma regime similar to that of an ionization chamber. On the other hand, the so-called ion guide systems are much smaller and only use gas flow to extract the ions[9,13].

Projectile fragmentation reactions occur at high incident energies, e.g.,  $\geq 100\text{MeV/u}$  and produce a very large variety of nuclei without decay or chemical losses. The products from these reactions are used at high energy to carry out much of current nuclear research [14]. The stopping and collection of projectile fragments is highly desirable but particularly difficult due to their long ranges and concomitant large range straggling even when range-compression techniques are used [15,16,17]. For example, the energy loss and range distributions of energetic  $^{68}\text{Se}$  projectile fragments used in this work are shown on the left side of Figure 1. Large range straggling implies that the stopped projectile fragments will always have to be collected from a large spatial region with significant primary ionization. The calculated residual energy of a fast ion that would be deposited in 1 bar of helium at the end of the range in a thickness equal to the full-width at half-maximum (FWHM) of the the range straggling distribution is shown on the right side of Figure 1. This estimate was made by obtaining the FWHM of the range distribution for a monoenergetic ion in helium gas from the well known *Stopping and Range Tables* [18] and then finding the kinetic energy of that ion with a range equal to the straggling FWHM. Figure 1 shows that the increase of deposited energy with incident energy is much larger than the variation with mass number. The figure also indicates that the effects of primary ionization will be much stronger for projectile fragments produced at 100 MeV/u or more than for nuclear recoils at a few MeV/u.

Given that the length of a gas cell for efficient collection and the amount of energy deposited per incident ion are dictated by the incident energy, it is important to consider the effects of space charge and ion recombination on the collection of thermalized ions in gas. Huyse et al. identified the density of ionization created by the stopping ion as an important parameter to describe the general behavior of the system as opposed to the simple rate of impinging particles [19]. The ionization-rate density used in the following discussion is the quotient of the rate at which ion-electron pairs (initially assumed to be  $e^-$  and  $\text{He}^+$ ) are created by the incoming radioactive ions and the stopping volume. Recombination processes place an overall limit on charge buildup in a gas cell. The remaining space charge affects the ion motion from the point where they stop to the extraction point as addressed in more detail by Takamine[11] and Schwarz[20]. Recombination is not important in linear gas cells under typical operating conditions and so the electrons can be rapidly removed leaving the space-charge from the cations to induce a radial field gradient that generally pushes the cations out of the ionization volume towards the walls during their longitudinal drift.

In the present work we describe the measurement and detailed simulations of cation

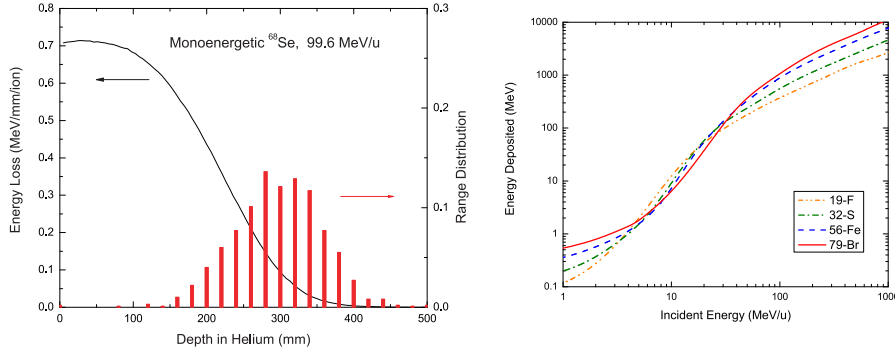


Fig. 1. (left) The energy loss and range distributions of monoenergetic  $^{68}\text{Se}$  ions at 99.6 MeV/u that pass through 2.200 mm glass, 0.566 mm beryllium and enter helium gas with a density of  $1.65 \times 10^{19}$  atoms/cm<sup>3</sup> calculated with the TRIM program[18]. (right) The calculated residual energy of a fast ion that would be deposited in the helium stopping gas at the end of the range in a thickness equal to the full-width at half-maximum of the the range straggling distribution is shown as a function of the incident kinetic energy.

collection from the NSCL gas cell. The results from the measurement of the extracted charge with a pulsed secondary beam were found to be in excellent agreement with particle-in-cell calculations of the ion migration. After describing the experiment we address the effects of the chemical evolution of the initial ionization in helium, an often neglected subject.

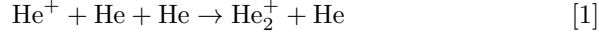
## 2. Ion Chemistry

As noted above, the slowing down of the nuclear recoils in gas creates a vast number of ion-electron pairs and the single incident ion is swept up in the evolution and migration of the buffer gas ions. The ion currents can be readily measured and used to monitor fast ion stopping in the gas cell as long as the space charge potential remains less than the applied potential. In this section, the general chemical nature of the migrating ions is presented first and then the level at which ion migration is affected by space charge along the lines presented by the Leuven group[19,13] is considered.

Fast nuclear recoils that are thermalized in helium gas are expected to remain ionized because the first ionization potential of helium is larger than that of any chemical element. However, significant chemical evolution of projectile fragments has been observed with the NSCL gas cell, e.g.,[8,1] whereas no ion-molecule chemistry and very few stable molecular ions have been observed to emerge from the SHIPTRAP gas cell [21] even though the state-of-the-art UHV and gas purification techniques are used in both systems. The properties of a prototype cryogenic gas cell were studied by Dendooven and cryogenic cooling of the gas may be an easier route to ultrahigh purity gas[22] but no full-scale cryogenic gas cells exist at present.

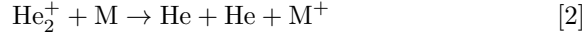
While it might be attractive to think that the helium stopping gas retains the ionization, we will show that the situation is more complicated. The initial ion chemistry of helium is somewhat simple since only three species are possible:  $\text{He}^+$ , its excited states, and the bare nucleus  $\text{He}^{2+}$ . As was pointed out some time ago by Patterson, all of the

$\text{He}^{2+}$  ions rapidly convert into  $\text{He}^+$  by two-body charge transfer reactions and the excited states of  $\text{He}^+$  rapidly decay leaving only ground state  $\text{He}^+$  ions[23,24]. However, a  $\text{He}^+$  ion will then go on to form the relatively stable dimer  $\text{He}_2^+$  by the reaction:

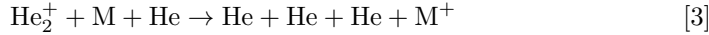


with a rate given by the expression:  $R = k_1 \rho_n^2$  in which  $\rho_n$  is the number density of (neutral) helium and  $k_1 = 1.08 \times 10^{-31} \text{cm}^6/\text{s}$  is the second order rate constant. Details of the formation of the ground and excited states of the helium molecular ion are not important for the present discussion. It is easy to show that the half-life for dimer formation is  $T_{1/2} = \ln 2 / (k_1 \rho_n^2) \sim 1 \mu\text{s}$  at a pressure of 100 mbar and only  $\sim 10 \text{ ns}$  at 1 bar at ambient temperature. In fact, it is very difficult to measure the ion mobility of  $\text{He}^+$  at pressures above a few mbar due to their rapid disappearance. Therefore, all of the primary helium ions produced in gas cells used to capture nuclear recoils are converted into  $\text{He}_2^+$  on a time scale that is small compared to that for ion drift in typical applied fields (10 V/cm).

It was also pointed out by Patterson and coworkers that “small traces of contaminants [in pure helium gas] become strongly preferentially ionized by charge transfer.”[24]. Recent calculations of chemical equilibria in noble gas plasmas show in detail that trace impurities rapidly become the significant charge carriers.[25] This conversion takes place by the two-body process (bimolecular reaction):



and is supplemented at high pressures by the three-body process (trimolecular reaction):



where M is *any* neutral impurity molecule. The chemical nature of the impurity, M, depends on the history and operation of the gas cell. For example, extensive studies of the output from the NSCL gas cell with a Penning trap mass spectrometer have shown that alkane and alcohol based molecular ions ( $\text{C}_2\text{H}_3^+$ ,  $\text{C}_2\text{H}_5^+$ ,  $\text{C}_4\text{H}_7^+$ ,  $\text{CH}_2\text{OH}^+$ ,  $\text{CH}_2\text{CH}_2\text{OH}^+$ , etc.) are strongly produced from the gas cell when it is only cleaned to “high vacuum” conditions; that water-based molecular ions ( $\text{H}_3\text{O}^+$ ,  $\text{H}_5\text{O}_2^+$ , etc.) are strongly produced shortly after an ultra-high vacuum (UHV) gas cell is exposed to air; and that fluorocarbon molecular ions ( $\text{CF}_3^+$ ,  $\text{C}_2\text{H}_3\text{F}_2^+$ , etc.) are produced by a carefully prepared UHV gas cell connected to a helium purifier. For example, the mass spectrum of ions produced by a discharge in the gas cell just after the beam time is shown in Figure 2. Ions with a mass-to-charge ( $m/q$ ) ratio of approximately 40 to 80 were selected by the ion-guides and their masses were determined in a time-of-flight measurement. The prominent ions were identified by observing their resonances in a Penning Trap mass spectrometer.

The rate constants for bimolecular charge exchange,  $k_2$ , (Eq. 2) are approximately  $\sim 2 \times 10^{-9} \text{cm}^3/\text{s}$  for a variety of small molecules including  $\text{C}_3\text{H}_8$  and  $\text{CCl}_2\text{F}_2$ . The rate constants for trimolecular charge exchange,  $k_3$ , (Eq. 3) with these two molecules are approximately  $2 \times 10^{-30}$  and  $8 \times 10^{-30} \text{cm}^6/\text{s}$ , respectively[26]. The mean lifetime for a  $\text{He}_2^+$  ion in the presence of trace amounts of propane (M) is simply  $\tau = 1/(k[\text{M}])$  where  $k = k_2 + k_3[\text{He}]$  and square brackets indicate concentrations. The mean lifetime at ambient temperature is shown in Fig.3 as a function of propane pressure in a helium

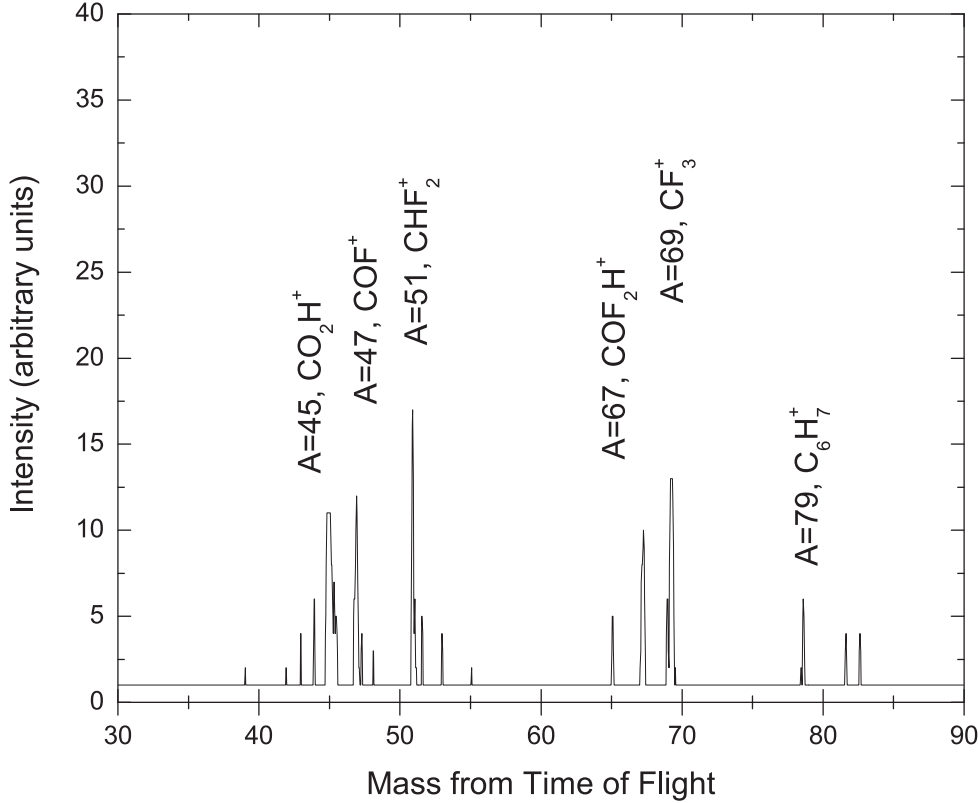


Fig. 2. The time-of-flight mass spectrum of ions in the mass range  $\sim 40$  to  $\sim 80$  created by an electric discharge in the NSCL gas cell. Labels indicate specific ions that were identified by Penning Trap mass spectroscopy.

buffer at pressures of 0.1 and 1 bar. The rates for charge transfer to other impurities are similar. Note that charge transfer takes significantly more time at low impurity levels than helium dimer formation, thus the charge carriers evolve from  $\text{He}^+$  to  $\text{He}_2^+$  and then to  $\text{M}^+$  if the ions drift in the helium for sufficient time.

Currently available helium purifiers and standard UHV techniques can reduce the impurities in the buffer gas to the level of a few parts-per-billion (ppb). The mean lifetimes for charge exchange in helium at this purity level, highlighted in Fig.3, increases from approximately 17 ms to approximately 170 ms as the pressure decreases from 1.0 to 0.1 bar. These lifetimes should be compared to an estimate of the time that nuclear recoils spend drifting before extraction given by the expression  $t = \Delta x / (\mu E)$  where  $\Delta x$  is the path length,  $\mu$  is the pressure dependent ion mobility, and  $E$  is the net average electric field. The reason for the difference in the chemical evolution of the primary ionization in the NSCL and the SHIPTRAP gas cells is now apparent. The shortest drift time from the midpoint of the NSCL gas cell at 1 bar of  $t \sim 50$  ms ( $\mu \sim 20 \text{ cm}^2/\text{s/V}$  and  $E \sim 25 \text{ V/cm}$ , see for example, [27]), is longer than the mean lifetime for charge exchange at this pressure. On the other hand, the drift time reported for the SHIPTRAP gas cell of  $t \leq 10$  ms [21] is fifty times shorter than the estimated mean lifetime for reactions in

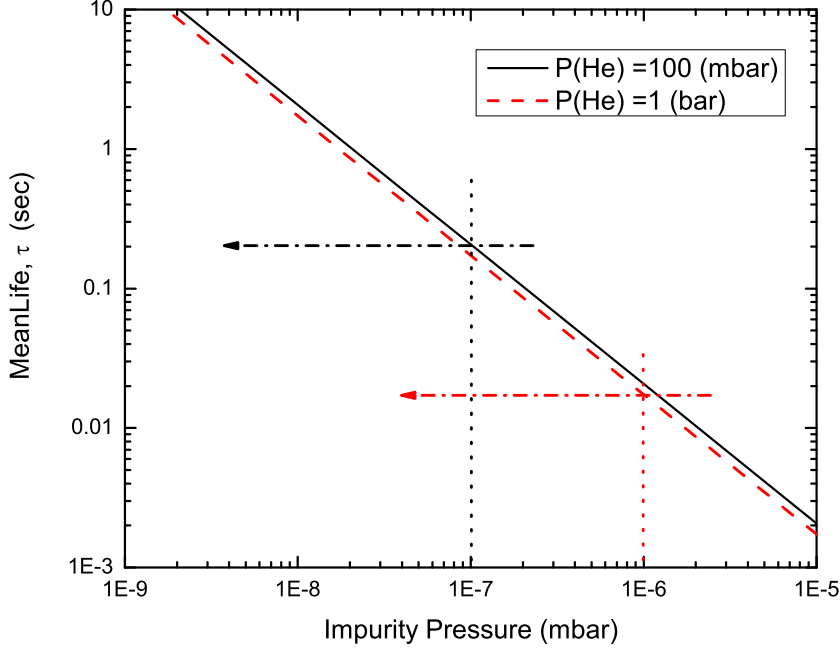


Fig. 3. The mean lifetime at ambient temperature for charge exchange between  $\text{He}_2^+$  and propane ( $\text{C}_3\text{H}_8$ ) as a function of propane pressure in bulk helium using the rate constants from Collins[26]. The dotted arrows indicate the expected lifetimes for 1 ppb propane in helium at two representative pressures.

this system ( $\tau \sim 500$  ms) at the same ppb level of contamination. The very low pressure (40 mbar) in this device speeds up the drift time and also lowers the rate of charge exchange of  $\text{He}_2^+$  with any impurities.

In summary, we expect that all of the primary ionization caused by the nuclear recoils will be converted into  $\text{He}_2^+$  ions within a timescale that is short compared to the extraction time of those recoils from any gas cell. The fate of the dimer ions depends on the level of molecular impurities in the gas and the drift time for the ions. Gas purifiers provide a uniform level of impurities per atom in the ppb range or in other words a relative residual gas pressure in the helium buffer gas. This uniform purity level does not insure a uniform amount of charge transfer from the  $\text{He}_2^+$  ions since a higher total pressure lowers the ion mobility, increases the drift time and also increases the charge transfer through an increased number of ion-molecule collisions.

### 3. Experimental

The present work used the high pressure gas-filled chamber (so-called “gas cell”) developed at the NSCL to thermalize, drift and extract high velocity projectile fragments

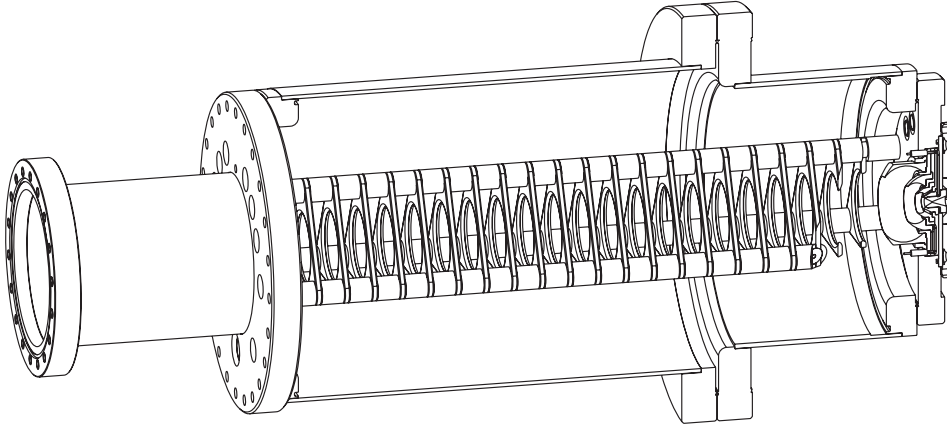


Fig. 4. A mechanical drawing of the NSCL gas cell with a cross section showing the drift rings, the spherical focussing electrodes and the nozzle. Fast projectile fragments enter from the left side and thermalized ions exit on the right.

before they can decay [7, and references therein]. Components of the fast-ion stopping system include a momentum-dispersive beam line with precision degraders (1.332 mm  $\text{SiO}_2$ ) and a precision wedge (0.729 mm at midpoint; borosilicate glass) for momentum compression of the projectile fragments upstream of the helium-filled gas cell. Degraded but still somewhat energetic ions enter the gas volume shown in Figure 4 (50 cm by 25 cm diameter) through a polished beryllium window (0.566 mm thick by 5 cm diameter) and are thermalized in ultra-pure helium gas. Collinear ring electrodes (inner diameter 5.6 cm) outside the stopping volume are used to create a DC gradient to drift all cations towards the exit, at which point four spherical electrodes are used to focus the ions on the exit nozzle (throat diameter 0.6 mm). Gas flow moves the ions toward and through the nozzle into a lower pressure ( $\sim 0.1$  mbar) chamber when the ions approach the throat of the nozzle. A differential pumping system removes the large amount of neutral helium gas leaving the gas cell while the ions are captured by a quadrupole ion guide that extends through the expansion chamber wall into a high vacuum region ( $\sim 10^{-6}$  mbar). The ions are then accelerated up to 5 keV for transport or measurement, see for example [28,29].

In the present work, a mixture of isotones with  $N=34$  was obtained from the A1900 projectile fragment separator[30] by the fragmentation of a 151 MeV/u  $^{78}\text{Kr}$  primary beam in a 331 mg/cm<sup>2</sup> beryllium target. The incident mixed beam contained:  $^{65}\text{Ga}$ ,  $^{66}\text{Ge}$ ,  $^{67}\text{As}$ ,  $^{68}\text{Se}$  in the proportion of 7:19:10:1 as determined by a combination of time-of-flight from the production target and energy loss in a silicon detector that could be positioned inside the gas cell 39 cm from the entrance. A continuous beam of ions was delivered by the NSCL facility but short beam pulses (2 ms), created by manipulating the rf-phase in the K500 accelerator, were also used to study the ion migration.

During the ion-current measurements the secondary beam was slowed down in the precision  $\text{SiO}_2$  degraders and wedge and the ions were thermalized in ultra-high purity helium at a pressure of 650 mbar. The effective thickness of the glass degraders was

varied by rotation. The ratio of ions stopped in the chamber to the number of incident ions was measured as function of the degrader thickness using the silicon detector both with and without filling gas. The point-by-point difference between these measurements, shown and discussed below, provided the range distributions of the ions. After the range measurements were complete the silicon detector was removed from the active volume.

#### 4. Ion Currents

Several measurements of the ion currents created by the fast beam were obtained in the present work. As indicated above, the stopping profile or essentially the range distribution of all of the incident ions was measured in the silicon detector. The results are shown by the squares in Fig.5. The stopping profile was also calculated with the TRIM code[18] using information on the transverse and longitudinal momenta of the mixed secondary beam at the degrader position predicted by a LISE++ simulation[31]. The predicted range distribution has no free parameters and the centroid was brought into the agreement shown in Fig.5 by decreasing the absorber thickness by only  $60\text{ }\mu\text{m}$  out of a total thickness of  $2685 \pm 8\text{ }\mu\text{m}$ . This discrepancy is within the uncertainty of the momentum measurement of the fragment distribution from the A1900 separator itself. The observed distribution in Figure 5 is slightly narrower than the calculated distribution which may be due to an overestimate of the acceptance of the system in the LISE++ simulation. Note that 50 cm of helium at 650 mbar is equivalent to  $25\text{ }\mu\text{m}$  of this glass so that essentially all ions of any one of the incident isotopes can be stopped in the gas when the degrader is centered on the maximum of each curve in Fig.5.

##### 4.1. Electrons and Negative Ions

After the silicon detector was removed, a voltage distribution was applied to electrodes inside the gas to separate the ion-electron pairs. Electrons and any anions were collected at high potential on the third ring (counting from the entrance window) while the cations were drifted toward the extraction nozzle that was near ground potential. The drift field was approximately constant at  $\sim 4\text{ V/cm}$ , approximately  $0.025\text{ Td}$ , at a pressure of 650 mbar. The negative ion current was measured by an electrometer connected to the third ring electrode that was at a slightly higher potential than its neighbors. The gas cell was thus behaving like a gas-filled ionization chamber (Bragg geometry) in which the incident ions leave a fraction of their incident energy in the gas whenever the glass is too thin to have the ions stop in the gas.

The negative ion current was obtained in DC mode as a function of degrader thickness and divided by the incident fast-ion rate and by the effective ionization potential of helium (42 eV) to produce the ionization profile shown in Fig.6. The typical incident rate during this measurement was  $10^4\text{ ions/s}$ . The ionization profile as a function of degrader thickness is a measurement of the Bragg curve when the negative ion collection is complete. For comparison, the Bragg curves were calculated as function of the glass degrader thickness for each ion type in the gas cell with the TRIM code using the input from the LISE++ simulations. The experimental results and the total ionization predicted for the mixed beam are shown in Fig.6. Once again there is excellent agreement between the total theoretical ionization and the experimental measurement. In the present case each



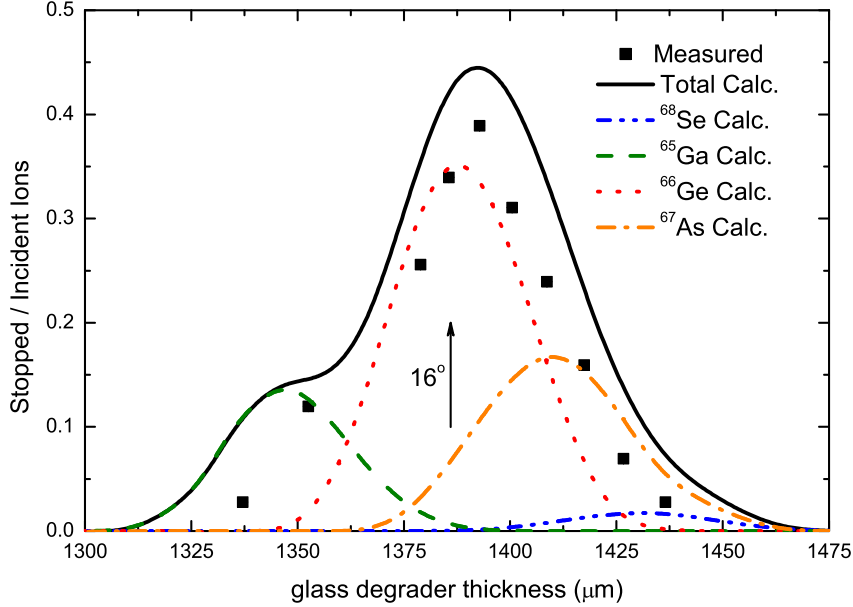


Fig. 5. The experimental (squares) and theoretical (lines) fraction of incident heavy ions stopped in a 39 cm long path at  $p=650$  mbar are shown as function of the degrader thickness. In addition, the calculated contributions from each species in the cocktail beam are indicated, see the text for details. The glass thickness at an angle of  $16^\circ$  is indicated for reference.

incident ion creates approximately  $5 \times 10^6$  ion-electron pairs during the stopping process that are distributed along a column. The stopping volume containing the ionization for all of the fast ions was estimated to be  $58 \text{ cm}^3$  from the range and diameter of the incident beam. Such large numbers of ion-electron pairs is typical for projectile fragments when a substantial fraction of the range distribution is collected, as discussed above.

#### 4.2. Positive Ions

The ion current due to the positive ions (cations) from the NSCL gas cell can only be measured after the nozzle and thus outside the gas cell. The measurement and interpretation of the cation current is complicated by the ion chemistry occurring during the drift time and by any mass selection in the ion guides after the nozzle. In order to study the behavior of extracted ions from the gas cell, 2 ms long pulses of secondary beam were injected into the gas cell. This pulse width is small compared to the drift time of the cations but provides enough ionization for the measurements. The time profile of positive ions exiting the gas cell after the beam pulse was recorded with a digital oscilloscope connected to a microchannel plate (MCP) detector placed several meters downstream from the ion guides. The MCP intercepted the ions after they passed through the ion

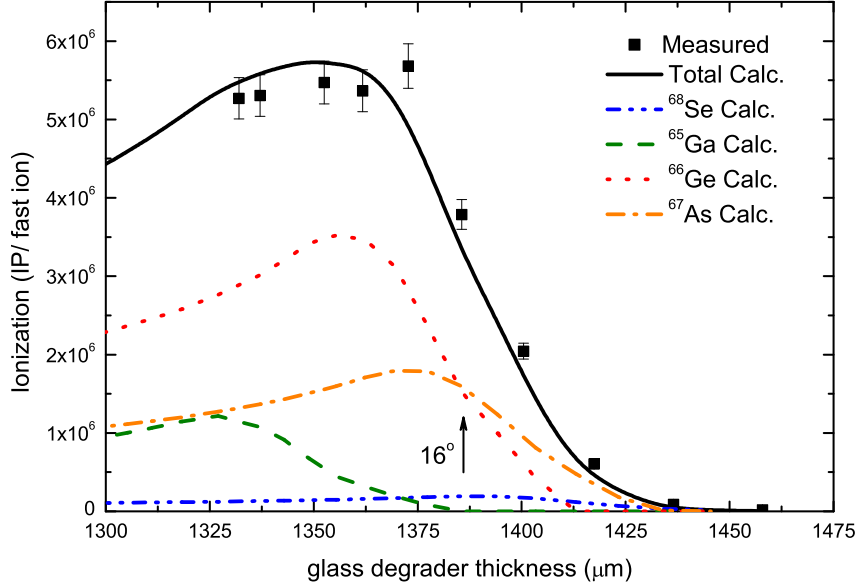


Fig. 6. The measured (squares) and theoretical (solid line) ionization profile from the negative ion current (in ion-electron pairs/incident ion) is shown as function of glass degrader thickness. The contributions from each projectile fragment is shown, similar to Figure 5.

guides and were accelerated to  $\sim 5$  kV. The next beam pulse was injected into the gas cell only after a pause to transfer the data from the oscilloscope.

Examples of the measured time profiles are shown in Fig.7 (dots) for an incident beam intensity of  $2.7 \cdot 10^4$  pps with the glass degrader, 1.332 mm thick, tilted to either (a)  $16^\circ$  or (b)  $18^\circ$  with respect to the normal to the beam direction. The projectile fragments travel the entire length of the gas cell under these conditions, see Fig.5, and stop in the central spherical electrodes. The columns of ion-electron pairs contain approximately  $1.9 \cdot 10^8$  and  $2.7 \cdot 10^7$  IP per projectile fragment (PF) distributed along the entire central axis which would correspond to ion pair densities of approximately  $3.3 \cdot 10^6$  and  $4.7 \cdot 10^5$  ion-electron pairs/cm<sup>3</sup>/PF. Recall that these densities are sufficiently low that recombination can be neglected. Following the discussion of charge exchange processes above, we expect that all of the electrons will be rapidly collected on the ring anode and that all of the positive charge will be transferred to impurity molecules before leaving the gas cell given their long drift times.

The ion guides were set to transmit mass-to-charge ( $m/q$ ) values in the range of approximately 40 to 80. The composition of this ion beam was not measured during the beam time but the results of many studies of the ion output from the NSCL gas cell indicate that it consists mainly of hydrocarbon molecular ions and small fluorinated hydrocarbons, see Figure 2 and discussion above. Thus, we expect the bulk of the cations extracted from the gas cell to be transmitted to the MCP detector and recorded. The

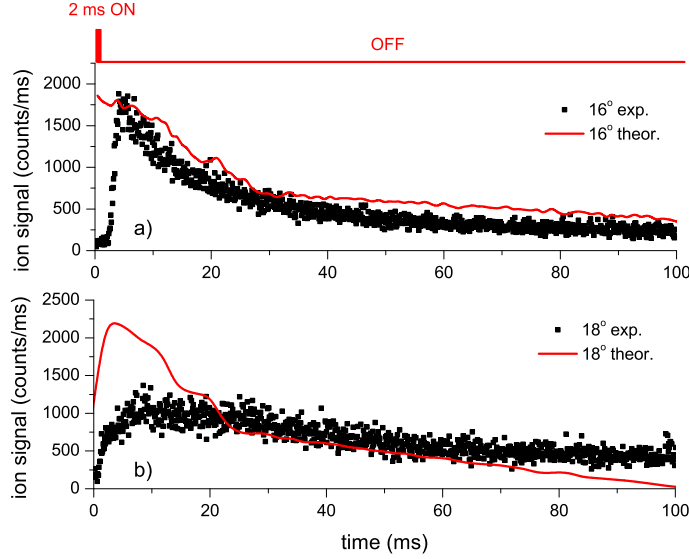


Fig. 7. Measured (dots) and calculated (line) time profiles of positive ions extracted from the gas cell after a beam pulse enters the gas cell and the glass degrader is positioned at either (a)  $16^\circ$  or (b)  $18^\circ$ . The primary ionization was created by 54 incident projectile fragments created in 2 ms and was drifted with 0.01 ms time steps.

observed time distributions peak at short times and then have an exponential tail. The observed time scales are consistent with simple expectations and detailed calculations of the ion migration are discussed in the next section.

The measured total extraction efficiency of molecular ions was obtained from the ratio of the Integral of the measured time profiles from Fig.7 of the extracted ions to the total number of molecular ions from the primary ionization. This efficiency turns out to be  $5 \cdot 10^{-4}$  for the  $16^\circ$  data and  $6 \cdot 10^{-4}$  for  $18^\circ$  data. These ratios include losses due to the extraction efficiency, the transport efficiency in the ion guides and the detection efficiency. The transport efficiency was estimated to be 0.2(1) by measuring total ion current at various points along the ion guides and beam line. Unfortunately the MCP was run in a analogue mode and the constant of proportionality was not measured so that the extraction efficiency could not be determined.

#### 4.3. Particle-in-cell Calculations

The detailed ion migration in the gas cell will depend on the combined effects of the applied field, the space charge of the ions and finally by gas flow in the region of the nozzle. The removal of the electrons and creation of a net positive charge in the gas cell leads to an increase of the potential in the gas cell, which counteracts the applied field[19] even in the case of a short pulse of ionization[32]. A particle-in-cell (PIC) code was developed to model the ion motion in this situation using cylindrical symmetry[33] without the effects of gas flow. The few projectile fragments that created the primary

ionization were placed in the gas volume according to their calculated range distributions, Fig. 5 and the much more numerous  $\text{He}_2^+$  ions were placed according to the calculated ionization distribution, Fig. 6. The ion mobilities of all of the cations in helium are only approximately twice that of  $\text{He}^+$  (which has a very short half life, discussed above) so that the chemical nature of each ion is not important. The migration of all of these ions was then tracked as a function of time from their creation until extraction or loss at the electrodes and/or boundaries and the drift time was recorded.

The absolute time distributions of the extracted molecular ions after the beam pulse are shown by the solid lines in Fig.7 for different glass degrader thicknesses. Small wiggles in the calculated curves are indications of the statistical accuracy of the calculations. The calculated results are in good general agreement with the observations and reflect the interplay of the shape of the drift field and the radial expansion due to the space charge. Recall that the geometry of the gas cell is such that there is a radial component to the applied field only in the region of the spherical electrodes. The time distribution observed with the thinner degrader (a more uniform column of ionization) is more sharply peaked in the data than in the calculations. This time peak is created by the *loss* of ions at longer times due to the expansion of the ion cloud in the region of the ring electrodes. In fact,

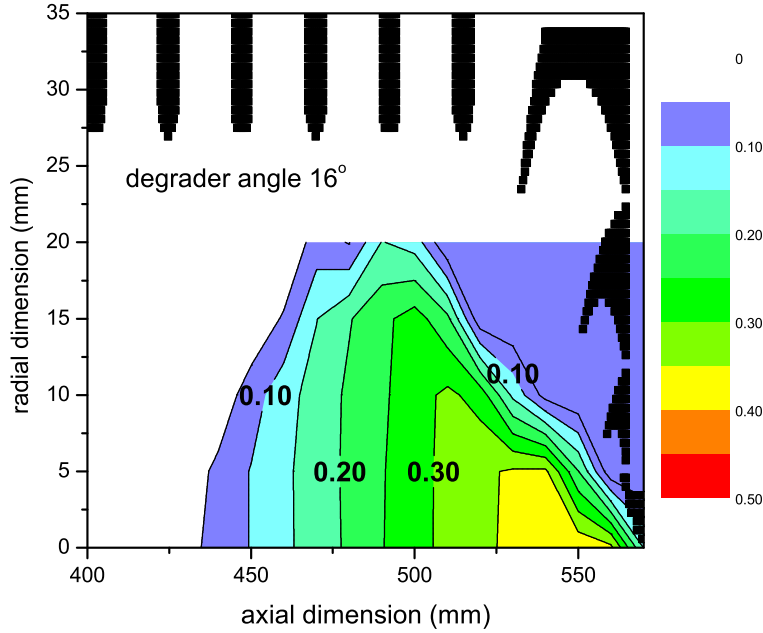


Fig. 8. Density plot of extraction probabilities of molecular ions from the gas cell when the rotation angle of the glass degrader was  $16^\circ$ . The black shapes along the edge indicate the positions of the spherical electrodes and the ring electrodes numbers 16 to 21.

only ions created relatively close to the extraction region are collected (see below). The more gradual rise and fall of the number of extracted ions in the case of lower ionization is only generally reproduced by the calculations due to the fact that the primary ionization is higher in the region further from the extraction region.

The extraction probability was obtained for each grid element by following the trajectories of ions placed at each of the nodes of the PIC grid. The extraction probability is the ratio of the number of ions that entered the throat of the nozzle electrode to the total number of initial ions. The resulting values were very similar for the two cases and the values for the  $16^\circ$  degrader angle are shown in Fig.8. The extraction probability has a maximum of approximately 50% for ions created near the nozzle and drops to near zero for ions created more than 10 cm upstream. Recall that this simulation does not include forces due to gas flow that would increase the extraction efficiency near the nozzle.

The predicted extraction probability of molecular ions can be determined by folding the extraction probabilities shown in Figure 8 with the initial ion distribution. Note that the calculations indicated that no ions would be extracted outside the volume indicated in Figure 8. In the present case the ionization distribution was approximately uniform over a column of  $123\text{ cm}^3$  because the radioactive beam did not stop in the gas. Combining these distributions one obtains a predicted extraction probability of 8% that is dominated by the region near the nozzle. This value of a few percent is similar to the values previously reported for the extraction of radioactive ions injected into the NSCL gas cell at low rates[7].

## 5. Summary and Conclusions

The fates of various ions created by the injection of pulses of projectile fragments into the NSCL gas cell were considered. A discussion of the gas phase chemistry indicated the importance of charge exchange reactions for conversion of the primary ions ( $\text{He}_2^+$ ) into various molecular ions. The lifetimes for these charge exchange reactions are such that all of the primary ionization will be transferred to molecules before extraction in this system. This conversion essentially increases the mass of the moving ions from  $A=8$  into the mass region of the injected projectile fragments and obviates mass-selection against the primary ionization in this case.

The measured distributions of the incident ions and the primary ionization were shown to be in excellent agreement with the predictions. A Particle-In-Cell code was developed to describe the motion of the positive ions in the gas cell including a self-consistent space charge. The results of the calculations are in good general agreement with the experimental data.

The assistance of the LEBIT group during the acquisition of the time spectra is gratefully acknowledged. This work was supported in part by the US Department of Energy under grant DE-FG02-00ER41144 and by the US National Science Foundation Grant PHY-06-06007.

## References

- [1] M. Block, *et al.*, Phys. Rev. Let. **100** (2008) 132501.
- [2] T. Eronen, *et al.*, Phys. Rev. Let. **100** (2008) 132502.
- [3] J.A. Clark, *et al.*, Phys. Rev. C **75** (2007) 032801.
- [4] T. Nakamura, *et al.*, Phys. Rev. A **74** (2006) 052503.
- [5] X. Wu, *et al.*, Proc. 2007 Particle Accelerator Conference, C. Petit-Jean-Genaz, Ed., IEEE Publishing, New Jersey, 2007, 1769.
- [6] S. Schwarz, G. Bollen, M. Kostin, F. Marti, P. Zavodszky, J.R. Crespo Lopez-Urrutia, J. Dilling, and O. Kester, Rev. Sci. Instrum. **79** (2008) 02A706.
- [7] L. Weissman, *et al.*, Nucl. Instrum. Meth. Phys. Res. **A540**(2005) 245.
- [8] G. Bollen, *et al.*, Phys. Rev. Let. **96** (2006) 152501.
- [9] J. Huikari, P. Dendooven, A. Jokinen, A. Nieminen, H. Penttilä, K. Peräjärvi, A. Popov, S.Rinta-Antila, and J. Äystö, Nucl. Instrum. Meth. Phys. Res. **B222** (2003) 632.
- [10] G. Savard, *et al.*, Nucl. Instrum. Meth. Phys. Res. **B204** (2003) 582.
- [11] A. Takamine, *et al.*, Rev. Sci. Instrum. **76** (2005) 103503.
- [12] J.B. Neumayr, *et al.*, Nucl. Instrum. Meth. Phys. Res. **B244** (2005) 489.
- [13] M. Facina, B. Bruynel, S. Dean, J. Gentens, M. Huyse, Y. Kudryavtsev, P. Van den Bergh, and P. Van Duppen, Nucl. Instrum. Meth. Phys. Res. **B226** (2005) 401.
- [14] D.J. Morrissey and B.M. Sherrill, Lect. Notes Phys. **651** (2004), 113.
- [15] H. Weick, *et al.*, Nucl. Instr. and Meth. Phys. Res. **B164-165** (2000) 168.
- [16] C. Scheidenberger, *et al.*, Nucl. Instr. and Meth. Phys. Res. **B204** (2003) 119.
- [17] L. Weissman, D.A. Davies, P.A. Lofy, and D.J. Morrissey, Nucl. Instrum. Meth. Phys. Res. **A531** (2004) 41.
- [18] SRIM2006 package by J.F. Ziegler and J.P. Biersack, <http://www.srim.org>.
- [19] M. Huyse, M. Facina, Y. Kudryavtsev, P. Van Duppen, and ISOLDE Colaboration, Nucl. Instrum. Meth. Phys. Res. **B187** (2002) 535.
- [20] S. Schwarz, private communication.
- [21] S.A. Eliseev, *et al.*, Nucl. Instr. Meth. Phys. Res. **B258** (2007) 479.
- [22] P. Dendooven, S. Purushothaman, and K. Gloos, Nucl. Instr. Meth. Phys. Res. **A558** (2006) 580.
- [23] P.L. Patterson, Phys. Rev. **A2** (1970) 1154.
- [24] E.C. Beaty and P.L. Patterson, Phys. Rev. **137** (1963) A346.
- [25] T. Martens, A. Bogaerts, W.J.M. Brok, and J.V. Dijk, Appl. Phys. Lett. **92** (2008) 041504.
- [26] C.B. Collins and F.W. Lee, J. Chem. Phys. **68** (1978) 1391
- [27] D.A. Davies, D.J. Morrissey, G. Bollen, P.A. Lofy, S. Schwarz, and J. Ottarson, Nucl. Instrum. Meth. Phys. Res. **A569** (2006) 883.
- [28] R. Ringle, *et al.*, Phys. Rev. **C75** (2007) 055503.
- [29] P. Schurry, *et al.*, Phys. Rev. **C75** (2007) 055801.
- [30] D.J. Morrissey, B.M. Sherrill, M. Steiner, A. Stolz, and I. Wiedenhöver, Nucl. Instrum. Meth. Phys. Res. **B204** (2003) 90.
- [31] O. Tarasov and D. Bazin, Nucl. Phys. **A 746** (2004) 411c, and references therein.
- [32] C. Velissaris, Nucl. Instr. Meth. Phys. Res. **A547** (2005) 511.
- [33] M. Facina, G. Bollen, and D.J. Morrissey, Hyperfine Interact **174** (2007) 21.